Characterization of Li_2O-Al_2O_3-SiO_2 glass-ceramics produced from a Brazilian spodumene concentrate

(Caracterização de vitrocerâmicas do sistema Li_2O-Al_2O_3-SiO_2 produzidas a partir de concentrado de espodumênio brasileiro)

L. B. Rebouças[1], M. T. Souza[1]*, F. Raupp-Pereira[1], A. P. Novaes de Oliveira[1]
[1]Federal University of Santa Catarina, Department of Mechanical Engineering, Laboratory of Glass-Ceramic Materials, 88040-900, Florianópolis, SC, Brazil

Abstract

Glass-ceramics in the LAS (Li_2O-Al_2O_3-SiO_2) system with high thermal shock resistance were successfully obtained using Brazilian spodumene concentrate as the main raw material (80-70 wt%). Two compositions ($Li_2O.Al_2O_3.nSiO_2$) were produced with n= 2 and 4, near to the stoichiometric compositions of β-eucryptite and β-spodumene. The characteristic temperatures of parent glasses were determined by contact dilatometry, differential scanning calorimetry and heating microscopy. The crystallization mechanism and the effect of the nucleating agent ($TiO_2.2ZrO_2$) required to promote volume crystallization in the parent glasses were investigated. Microstructural and structural changes with temperature were also evaluated by optical microscopy and X-ray diffraction. The obtained glass-ceramics presented coefficients of thermal expansion between $-0.370x10^{-6}$ and $4.501x10^{-6}$ °C^{-1} in the 22 to 700 °C range.
Keywords: Brazilian spodumene, glass-ceramics, thermal shock resistance.

Resumo

Vitrocerâmicas do sistema LAS (Li_2O-Al_2O_3-SiO_2) com elevada resistência ao choque térmico foram obtidas com sucesso com o uso de um concentrado de espodumênio brasileiro como principal matéria-prima (80%-70% em massa). Duas composições ($Li_2O.Al_2O_3.nSiO_2$) foram produzidas com n= 2 e 4, próximas às composições estequiométricas das fases eucriptita-β e espodumênio-β. A determinação das temperaturas características dos precursores vitrocerâmicos (vidros) foi realizada por dilatometria de contato, calorimetria de varredura diferencial e microscopia de aquecimento. O mecanismo de cristalização e o efeito do agente nucleante ($TiO_2.2ZrO_2$) necessário para promover a cristalização volumétrica das matrizes vítreas foram investigados. As alterações microestrutural e estrutural com a variação da temperatura foram também avaliadas por microscopia óptica e difração de raios X. As vitrocerâmicas obtidas apresentaram coeficientes de expansão térmica linear entre $-0,370.10^{-6}$ e $4,501.10^{-6}$ °C^{-1} no intervalo de 22 a 700 °C.
***Palavras-chave**: espodumênio brasileiro, vitrocerâmicas, resistência ao choque térmico.*

INTRODUCTION

The unique properties of lithium such as remarkable electrochemical reactivity and extreme lightness find innumerous applications in several engineering fields. With few feasible substitutes in sight, the lithium global market is mostly driven by the growing demand for lithium batteries for portable electronic devices and electric vehicles (Fig. 1), followed by ceramic and glass, lubricant and grease and several other applications, including nuclear power plants and military applications [1-5]. There are many mineral sources of lithium such as closed-basin brines, pegmatites and related granites, lithium-enriched clays, oilfield brines, geothermal brines and lithium-enriched zeolites [6]. In Brazil, lithium sources are usually found in hard-rock ore deposits in igneous pegmatite formations, especially in the States of Minas Gerais (MG) and Ceará (CE). Industrial mining is carried out exclusively in the Northeastern of MG (in the districts of Araçuaí and Itinga) by the Companhia Brasileira de Lítio, CBL (Brazilian Lithium Co.). In pegmatite deposits, Li-bearing aluminosilicate minerals, such as amblygonite, spodumene, petalite and lepidolite can be found. Among them, spodumene attracts great interest due to its high lithium content [7]. In 1974, Brazil imposed legal restrictions to control the use of lithium products aiming to protect the national resources from foreign speculation [8]. The idea was to position the country as one of the main lithium mineral explorers of the international and national market, dealing with beneficiation of lithium

* https://orcid.org/0000-0002-7831-4451

minerals as well as manufacturing of final lithium-based products. However, despite the worldwide lithium demand has increased at an average growth rate of 4% per year since 2005 [5], the demand for Brazilian lithium products is underwhelming. Even though Brazil has the available infrastructure for spodumene mining and production of lithium's hydroxide and carbonate, the last available mineral summary from the National Department for Mineral Production (DNPM) dated 2014 revealed that the apparent consumption of lithium chemical compounds declined 5.8% [9]. The main reason comes from the low-purity grade of Brazilian spodumene, making it hard to obtain high purity lithium compounds. In fact, the lithium compounds produced in Brazil still do not meet the specifications for battery-grade products required to produce primary lithium batteries (which are respectively 99.5% and 56.5% for lithium carbonate and lithium hydroxide) and for military purposes such as weapons or even as cooling additive for nuclear reactors [10]. Besides, due to the legal restrictions, the importation of lithium chemical compounds is limited to 20 kg per year per company [11]. Thus, the low purity grade of Brazilian spodumene and the lack of application diversity limits the use of Brazilian lithium compounds to lubricant and greases, which are applications with lower added value. In fact, lubricant and greases are responsible for more than 90% of Brazilian lithium product market [12].

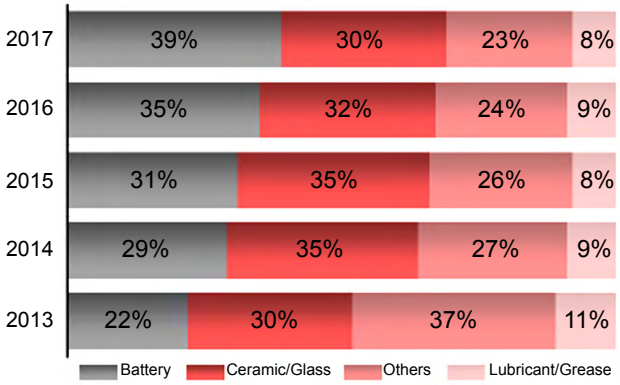

Figure 1: Global end-use markets of lithium products data from USGS' annual reports over the years 2013-2017 [1-5].
[Figura 1: Dados dos relatórios anuais do USGS do mercado global dos consumidores finais de produtos de lítio nos anos de 2013 a 2017 [1-5].]

On the other hand, the worldwide demand for low-purity lithium minerals is still significant and not only for the production of lubricant and grease, but also for the production of glass-ceramics. The glass and ceramic industry is the second largest share of lithium's end-use market. Despite Brazilian glass industries have global importance with a well-consolidated industry and know-how technology as well as many researches published by Brazilians (e.g. [13-17]), there are few records of industrial-scale production of glass-ceramics in Brazil. The chemical composition of Brazilian spodumene matches with the purity requirement and chemical composition of glass-ceramics of the Li_2O-Al_2O_3-SiO_2 (LAS) system. LAS system-based glass-ceramics are examples of engineered materials that attract great commercial interest. Due to their low thermal expansion (often close to zero), LAS glass-ceramic has been widely used for more than 60 years in telescopes mirrors [18], optical precision systems [19], cooktops [20], cookware [21], fireproof doors [22], heatproof windows [23], and heat exchangers [24]. This ternary system is based on two crystalline phases: β-eucryptite, a stuffed structure derived from the hexagonal high-quartz (often referred as β-quartz$_{ss}$ or virgilite) with coefficient of thermal expansion as low as -11 up to 1.7 x10^{-6} °C^{-1} [25], and β-spodumene, a solid solution derived from keatite with a coefficient of thermal expansion in the 1 to 2 x10^{-6} °C^{-1} range [26]. Lithium aluminosilicate solid solutions are obtained by heat-treating a parent glass of general composition Li_2O-Al_2O_3-nSiO_2 in which n ranges from 2 to 10. Monolithic glass-ceramics such as the LAS system can be produced by any conventional glass-forming technique with zero or very low porosity by using a source of alumina (Al_2O_3), quartz (SiO_2) and Li_2CO_3 or by the straight use of spodumene concentrate as a lower cost option, which is a simultaneous source of Li_2O, Al_2O_3 and SiO_2 [11]. Yet, some pure raw materials might be added to achieve the required stoichiometry.

Considering the costs of Brazilian lithium products and importation restrictions, spodumene concentrate might be a feasible option for a national LAS glass-ceramic raw material. Its concentration involves far less beneficiation steps than the production of high-purity lithium compounds. Therefore, this paper aims to evaluate the use of Brazilian spodumene concentrate as a main raw material for the production of monolithic glass-ceramics. Data on the characterization regarding its amenability to glass-formation and crystallization as well as its potential as a raw material to produce glass-ceramics with high thermal shock resistance were also considered.

MATERIALS AND METHODS

Spodumene concentrate (SC) was supplied by Brazilian Lithium Co. (CBL). From the visual analysis, three distinct fractions could be observed in the as-received SC. For characterization purposes, samples of the observed fractions were manually separated. Analyses were carried out in powdered samples (~45 μm). X-ray fluorescence spectroscopy (XRF, Philips, PW 2400) was performed to determine the chemical composition of samples in combination with atomic absorption spectroscopy (AAS, Unican, 969), especially used to determine the lithium content (not detected in the XRF). True density was measured by He-pycnometry (Quantachrome, 1200E) and X-ray diffraction (XRD, Philips, X'Pert). XRD analyses were carried out using Ni filter and CuKα (1.5418 Å) at 40 kV and 30 mA. Scanning was performed at 0.02° step in the 5°-75° 2θ range. From differential scanning calorimetry (DSC, TA-Instr., SDTQ600), it was possible to assess the crystallization enthalpy of glass-ceramics as well as the

need of a nucleating agent to promote crystallization. Many works reported the use and efficiency of different nucleating agents in the Li_2O-Al_2O_3-SiO_2 glass-ceramic system [27-33]. According to them, titania combined with zirconia in a 1:2 molar ratio revealed great results. Thus, batches of SC glass and SC with 4 wt% TiO_2.2ZrO_2 were prepared. DSC experiments were carried out and the crystallization enthalpy was calculated for glasses produced with the as-received SC (powdered and bulk sample) and with the SC and nucleating agent (4 wt% TiO_2/ZrO_2). This assay indicated the preferential crystallization mechanism: surface or volume [34].

Based on the results obtained from chemical composition analyses of the as-received SC and the nucleating agent performance, the compositions for the synthesis of two glass-ceramics prepared with SC as the main raw material were designed close to the stoichiometry compositions of β-spodumene and β-eucryptite, which are phases known by their low thermal expansion. Fig. 2 depicts the pseudo-ternary position within the Li_2O-Al_2O_3-SiO_2 diagram of LAS-s (65.30SiO_2-16.33Al_2O_3-16.33Li_2O-1.36TiO_2-0.68ZrO_2 - close to the β-spodumene stoichiometry) and LAS-e (48.49SiO_2-24.24Al_2O_3-24.24Li_2O-2.02TiO_2-1.01ZrO_2 - close to the β-eucryptite stoichiometry). Batches were comprised of 80-70 wt% spodumene and PA reagent grade lithium carbonate (Synth), alumina (Vetec) and silica (Sigma-Aldrich); 4 wt% TiO_2 (Vetec) and ZrO_2 (Sigma-Aldrich) in 1:2 ratio were added as nucleating agent; 2 wt% of Li_2O in excess was calculated to compensate Li evaporation during melting. The as-received SC was dry crushed in a hammer mill (Servitech, 01058) with a 2 mm opening grill and further milled in a planetary ball mill (Servitech, CT242) for 20 min. The mean particle size of the powdered SC (D_{50} of 19 μm) was determined using a laser scattering particle size analyzer (Malvern, Mastersize 3000). Batches of ~100 g of the LAS-s and LAS-e compositions were dry mixed and homogenized in an alumina jar mill (Cienlab, CE-500/D) for 2 h. The prepared mixtures were placed in a 100 mL platinum crucible and melted at 1550 °C for 2 h in a bottom loading furnace (Jung, LF 0917). The melts were splat-cooled between two steel plates and annealed (Quimis, Q318M) for 30 min at 5 °C above the glass transition temperature (Tg), previously determined for each glass.

To verify the amorphous nature of the produced parent glasses, XRD (Philips, X'Pert) analyses were performed on powdered samples (>45 μm). Monolithic specimens with nominal dimensions of 20x5x5 mm^3 were prepared for contact dilatometry (Netzsch, DIL 402-C). In this case, glass transition temperatures (Tg) and softening temperatures (Ts) were obtained by change on the curve slope and by the abrupt inversion of the expansion caused by the penetration of the rod into the sample. Experiments were performed at a 10 °C.min^{-1} heating rate in a synthetic air atmosphere. The crystallization temperatures were obtained by differential scanning calorimetry (DSC, TA, SDTQ600) at 10 °C.min^{-1} heating rate under synthetic airflow of 100 mL.min^{-1}. Aiming to evaluate the composition variability and the

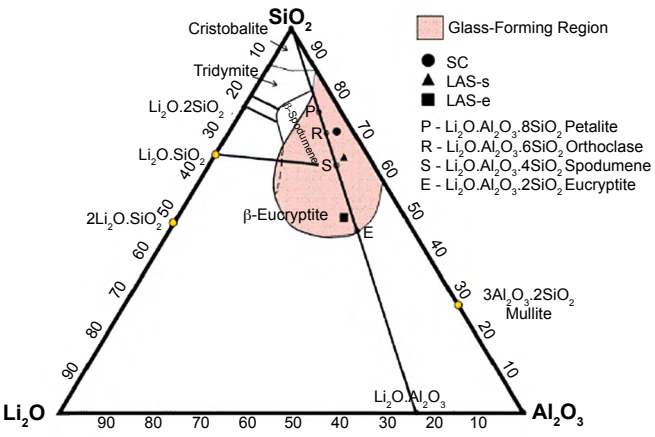

Figure 2: LAS system ternary phase diagram and the compositions of as-received spodumene concentrate (SC).
[Figura 2: Diagrama de fases do sistema ternário LAS e as composições do concentrado de espodumênio (SC).]

effect of residual oxides from the spodumene concentrate, the experimental thermal expansion coefficient (α) was also obtained from contact dilatometry curves for temperatures up to 400 °C and compared to the theoretical thermal expansion coefficients, α_T, calculated according to Appen [35]:

$$\alpha_T 10^7 = \frac{\sum \alpha_i a_i}{100} \quad (A)$$

where α_i represents the coefficient of thermal expansion and a_i the molar fraction of each constituent. X-ray fluorescence analysis (Philips, PW 2400) combined with atomic absorption spectroscopy (Unican, 969) was also carried out to determine the compositions of the produced parent glasses. The crystallization temperature was determined from the exothermic peak of differential scanning calorimetry (TA, SDT Q600) curves. The analysis was performed at a heating rate of 10 °C.min^{-1} and 100 mL.min^{-1} synthetic air flow. While direct viscosity measurement techniques, such as beam bending viscosimetry, display a characteristic increase on viscosity at crystallization temperature [36], the Vogel-Fulcher-Tammann (VFT) model [37, 38] does not consider the crystallization event. Nevertheless, Martendal and Oliveira [39] showed that applying the VFT equation from the experimental thermal analysis data, surface and volume crystallizations occur at characteristic viscosities (η). For surface crystallization, $\eta=10^{4.28\pm0.41}$ Pa.s, whereas the volume crystallization occurs at higher viscosity, $\eta=10^{6.37\pm0.51}$ Pa.s. From the results of thermal analysis, the viscosity curve as a function of the glass temperature can be calculated using the Vogel-Fulcher-Tammann model described by:

$$\text{Log}\eta = A + \frac{B}{T - T_0} \quad (B)$$

in which A, B and T_0 are calculated from Eqs. C, D and E, respectively, based on three characteristic temperatures and their respective viscosities, T_1=Tg (η=10^{12}), T_2=Ts (η=$10^{9.25}$) and T_3=Ths (η=$10^{3.5}$) or T_3=Tm (η=10^1) [40]:

$$T_0 = \frac{T_1\log\eta_1 - T_3\log\eta_3 + (T_2\log\eta_2 - T_1\log\eta_1)\frac{T_3-T_1}{T_2-T_1}}{\log\eta_1 - \log\eta_3 - (\log\eta_1 - \log\eta_2)\frac{T_3-T_1}{T_2-T_1}} \quad (C)$$

$$A = \frac{T_2\log\eta_2 - T_1\log\eta_1 + (\log\eta_1 - \log\eta_2)T_0}{T_2-T_1} \quad (D)$$

$$B = T_1 - T_0\,(\log\eta_1 - A) \quad (E)$$

Crystallization mechanism and crystal growth were also assessed through the Avrami model [41], which states that the degree of phase conversion (crystallization) under isothermal conditions is described by Eq. F. Upon the extraction of logarithms (Eq. G) a straight line is obtained. The Avrami exponent (n) can be deduced from the slope and k is given by the intercept of the straight line (Eq. G):

$$x(t) = 1 - e^{-kt^n} \quad (F)$$

$$\ln[\ln(1-x(t))] = \ln k + n \ln t \quad (G)$$

Experimentally, non-isothermal DSC runs in different heating rates are broadly used with few modifications to the Avrami original model. Jeziorny [42] proposed a replacement of the parameter k by k' which considers the heating rate (Φ), as shown in Eq. H. The crystallized fraction x was determined from the DSC crystallization peak according to Eq. I, in which dH/dT is the crystallization enthalpy at an infinitesimal temperature T (between T_0 and $T\infty$, initial and final temperatures of the event, respectively). x(T) is analog to x(t) where the reaction time t is given by Eq. J. A sigmoidal x(t) curve should be obtained. The data at the interval 20%<x<80% should fit a straight line by plotting Eq. G [43]. However, to ensure the applicability of the Jeziorny modification model aiming to describe the actual crystallization mechanism, the obtained data were compared with the viscosity approach to crystallization and later verified with the micrograph of heat-treated samples.

$$\ln k' = \frac{\ln k}{\Phi} \quad (H)$$

$$x(T) = \frac{\int_{T_0}^{T}\left(\frac{dH}{dT}\right)dT}{\int_{T_0}^{T_\infty}\left(\frac{dH}{dT}\right)dT} \quad (I)$$

$$t = \frac{T - T_0}{\Phi} \quad (J)$$

DSC (TA, SDT Q600) curves performed in monolithic samples (~20 mg) at 5, 10, 15 and 20 °C.min^{-1} with 100 mL.min^{-1} synthetic air flow were further used to obtain the apparent activation energy of crystallization by using the Kissinger method [44], shown in:

$$\ln\frac{T_p^2}{\Phi} = \frac{E_a}{RT_p} + C1 \quad (K)$$

where T_P is the temperature at crystallization peak and R=8.315 J.K^{-1}.mol^{-1} is the universal gas constant. Monolithic samples (~20 mg) were pre-treated for 2 h at different temperatures (T_N) between the parent glass Tg and Tc in a muffle furnace (EDG, F1800) and subjected to differential scanning calorimetry (TA, SDT Q600) performed at a heating rate of 15 °C.min^{-1} with 100 mL.min^{-1} synthetic air flow. It was assumed that the tendency of the nuclei concentration was the same as the inverse of the crystallization temperature as a function of the treatment temperature (T_N) [45]. The crystallization by heat-treatment was carried out in a muffle furnace (EDG, F1800) with a heating rate of 10 °C.min^{-1}. Based on the thermal analyses results, a two-step heat-treatment was defined with the first plateau at an optimal T_N for 2 h to maximize the number of nuclei in the glass matrix, followed by 2 h at temperatures above the crystallization peak temperature (Tc). The resulting microstructures were observed in a polarized light microscope (Leica, DM4000M) with 100x magnification. The crystalline phases were determined by X-ray diffraction (Philips, X'Pert) and identified with the aid of the Inorganic Crystal Structure Database (ICSD). Finally, the glass-ceramics were analyzed by contact dilatometry (Netzsch, DIL 402-C) at a heating rate of 10 °C.min^{-1} and 100 mL.min^{-1} synthetic air flow for determination of the coefficient of thermal expansion (α).

RESULTS AND DISCUSSION

The as-received SC (3.01 g.cm^{-3}) was previously processed through dense medium separation by CBL. This process is a well-known technique for separating particulate solids of different densities. Solid minerals are mixed with heavy liquids of suitable density, so that lighter density minerals naturally float while those denser sink. In this case, minerals with a density close to the spodumene are not effectively separated by using this process. From the as-received spodumene concentrate sample, it was possible to observe three distinct minerals. Fig. 3 shows photographs of the as-received spodumene concentrate sample and its constituent fractions (later named MS, MM and MQ). The densities of the three fractions were close to each other, with a variation of 0.24 g.cm^{-3} between them. In this case, it is worth noting that MS fraction measured density was 3.07 g.cm^{-3}, the closest to the theoretical α-spodumene mineral (3.11 g.cm^{-3}) [7]. Visual aspects were also closer to the green spodumene found in Brazilian pegmatites [6]. The MM fraction presented light iridescent shades, a lamellar fracture, and density of 2.83 g.cm^{-3}, whereas for MQ fraction with darker coloration, the measured density was 2.90 g.cm^{-3}. Characteristic peaks of spodumene (RRUFF ID: R050252.1), muscovite (RRUFF ID: R050080.1), and quartz (RRUFF ID: R050125.1) were identified in the as-received XRD pattern shown in Fig. 4a. Concentrate spodumene mineralogy revealed a mix of minerals, such

as spodumene, muscovite and quartz. These minerals were better evidenced at each separated fraction. The MS fraction presented characteristic peaks of α-spodumene (Fig. 4b). The XRD pattern of MM fraction revealed characteristic muscovite peaks (Fig. 4c) and the MQ fraction presented mainly quartz peaks (Fig. 4d).

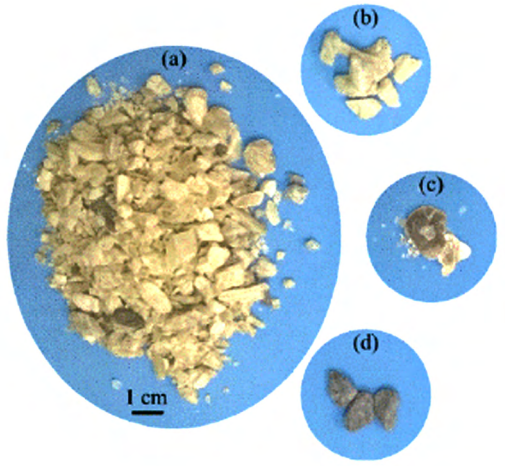

Figure 3: Photographs of as-received SC in the delivery state (a) and its constituent fractions MS (b), MM (c), and MQ (d).
[Figura 3: Fotografias de SC no estado de fornecimento (a) e suas frações constituintes MS (b), MM (c) e MQ (d).]

Chemical compositions are shown in Table I. The MS fraction was the main lithium carrier mineral composing the SC. According to chemical analysis, the SC was composed of roughly 48% of spodumene and the spodumene content in MS fraction was higher than 95%, evidencing a chemical composition similar to the theoretical spodumene (8.03% Li_2O, 27.40% Al_2O_3 and 64.58% SiO_2). The MM fraction was rich in potassium oxide and the composition was close to the theoretical muscovite (11.81% K_2O, 38.36% Al_2O_3, 45.21% SiO_2 and 4.07% H_2O). The higher loss on ignition (4.99 wt%) was also justified by the presence of H_2O in the muscovite structure. K, as well as Na and Mg (present in a higher amount in the fraction MQ), may lead to an increase in the coefficient of thermal expansion of the glassy phase and might have the same effect in the crystalline phase by substituting Li in the structure of β-quartz and β-spodumene decreasing the thermal shock resistance of the final product. On the other hand, up to a certain amount, the substitution might be desirable. In the manufacture of a commercial LAS

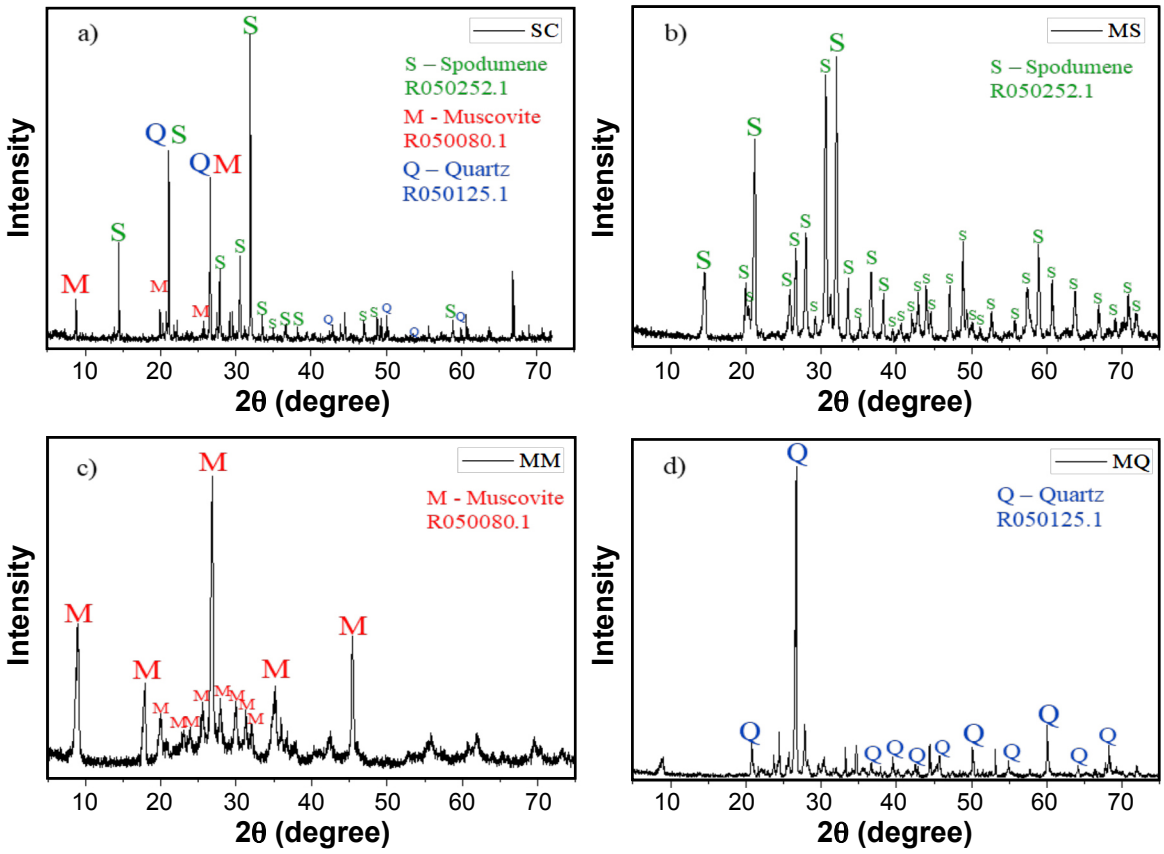

Figure 4: X-ray diffraction patterns of as-received mineral: a) SC with identified characteristic peaks of: S- α-spodumene (R050252.1), M- muscovite (R050080.1), and Q- quartz (R050125.1); b) MS fraction comprised of spodumene; c) MM identified as muscovite; and d) MQ fraction with identified characteristic peaks of α-quartz and at least a second-phase not identified.
[Figura 4: Difratogramas de raios X do mineral no estado de fornecimento: a) SC com picos característicos identificados de: S- espodumênio (R050252.1), M- muscovita (R050080.1) e Q- quartzo (R050125.1); b) fração MS composta por espodumênio-α; c) fração MM identificada como muscovita; e d) fração MQ com picos característicos identificados como quartzo-α e pelo menos uma segunda fase não identificada.]

glass-ceramic, CorningWare®, it was first reported that the partial substitution of a certain amount of Li_2O by MgO eliminated the appearance of spider webs in aluminosilicate glass-ceramics because it increased the temperature difference between nucleation and crystallization and reduced the viscosity of the glass during crystallization [46]. The MQ fraction contributed to the presence of Fe_2O_3 in the SC, which can act as chromophore oxide in the glass-ceramic. The presence of as little as 0.4 wt% of iron oxide in a glass composition can result in amber or brownish color to the final product. Iron oxide also reduces the linear transmission of infrared radiation [47], which would limit the use of this material in cooktops for infrared cooking. The visual sorting of the SC fractions demonstrated the possibility of obtaining a concentrate with a higher lithium content, but the results were still not as effective as other separation methods used in other countries. As an example, the reported lithium content of the Australian spodumene concentrate is 7 wt% [25].

Fig. 5 shows DSC curves performed in glasses produce from the as-received SC (powdered and bulk sample) and

Table I - Chemical compositions (wt%) of as-received SC and its constituent fractions MS, MM and MQ, obtained by XRF and AAS.
[Tabela I - Composições químicas (% em massa) do SC no estado de fornecimento e suas frações constituintes MS, MM e MQ obtidas por espectroscopias de fluorescência de raios X e absorção atômica.]

Oxide	SC	MS	MM	MQ
SiO_2	67.47	63.76	47.11	60.86
Al_2O_3	23.57	25.96	35.35	17.59
Li_2O	3.83	6.50	0.39	0.51
Na_2O	1.26	0.81	1,00	2.31
Fe_2O_3	1.02	0.51	1.39	5.69
K_2O	1.01	0.08	9.29	2.32
P_2O_5	0.26	<0.05	<0.05	1.15
CaO	0.24	0.21	<0.05	3.14
MgO	0.23	1.25	0.27	3.77
MnO	0.12	0.07	0.05	0.19
B_2O_3	<0.50	-	-	-
LOI	0.55	0.71	4.99	1.63

Note: BaO, Co_2O_3, Cr_2O_3, PbO, ZnO, ZrO_2, SrO, TiO_2 <0.1%.

from the SC with the nucleating agent (4 wt% TiO_2/ZrO_2). No exothermic peak was observed for the monolithic SC glass sample, whereas for the powdered sample, the crystallization initiated at ~870 °C (Tc=909 °C) with a crystal formation enthalpy of 103 $J.g^{-1}$. This behavior indicated that for glasses with the as-received SC, the surface crystallization was preferential. Therefore, the addition of a nucleating agent was required to provide bulk crystallization. The addition of 4 wt% $TiO_2.2ZrO_2$ yielded a crystallization at a lower temperature, with slightly higher crystal formation enthalpy, 110 $J.g^{-1}$. The nucleating agents promoted bulk nucleation and facilitated the crystallization process by reducing the crystallization temperature from 909 to 858 °C.

Fig. 6a shows a sample of LAS-s parent glass and Fig. 6b shows the XRD patterns for LAS-s and LAS-e parent

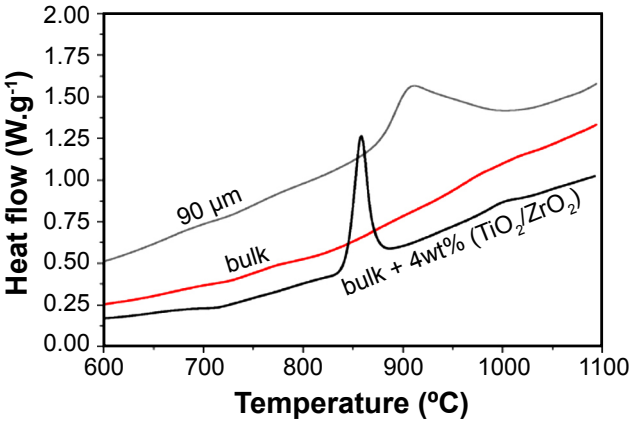

Figure 5: DSC curves showing the effect of adding 4 wt% of $TiO_2.2ZrO_2$ as a nucleating agent in glass prepared from SC.
[Figura 5: Curvas de DSC mostrando o efeito da adição de 4% em massa de $TiO_2.2ZrO_2$ como agente nucleante no vidro produzido a partir do SC.]

glasses. Both parent glasses were amber with homogenous coloration and transparent; the color was expected due to the chromophore role of Fe_2O_3 present in the SC composition. The absence of crystalline phases in the parent glasses after the splat-cooling and annealing was clearly observed by XRD patterns. LAS-s and LAS-e characteristic temperatures are shown in Fig. 7. The glass transition (Tg) and the softening (Ts) temperatures are indicated in the results of contact dilatometry (Fig. 7a) and the crystallization temperatures (Tc) are identified in the heat-flow curves shown in Fig. 7b. The two studied parent glasses showed a typical linear expansion behavior with an abrupt slope change at Tg followed by an apparent shrinkage actually caused by the penetration of the rod in the sample at Ts. Ts was lower for LAS-e especially due to the higher lithium content on its

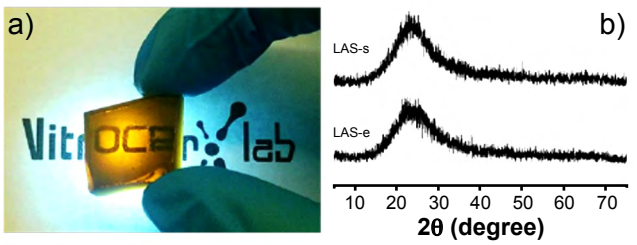

Figure 6: Photograph of the splat-cooled monolithic LAS-s parent-glass after annealing (a), and XRD patterns of LAS-s and LAS-e parent glasses (b).
[Figura 6: Fotografia do precursor vitrocerâmico LAS-s monolítico conformado por splat-cooling após recozimento (a) e padrões de DRX dos precursores vitrocerâmicos LAS-s e LAS-e (b).]

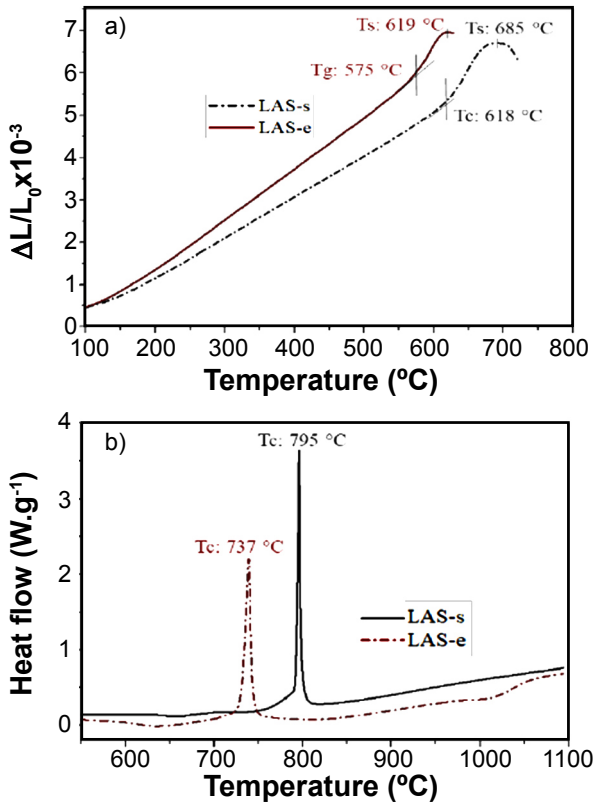

Figure 7: Linear thermal expansion curves with glass transition, Tg, and softening, Ts, temperatures (a), and heat flow curves with crystallization temperature, Tc (b), of LAS-s and LAS-e parent glasses.
[Figura 7: Curvas de expansão térmica linear com as temperaturas de transição vítrea, Tg, e de amolecimento, Ts (a), e curvas de fluxo de calor com as temperaturas de cristalização, Tc (b), dos precursores vitrocerâmicos LAS-s e LAS-e.]

chemical composition, which acted as a network modifier reducing the softening and melting temperatures. The crystallization temperatures of both parent glasses were characterized by single exothermic events evidenced at 737 °C for LAS-e and 795 °C for LAS-s.

Table II summarizes the measured thermal and physical properties of LAS-s and LZS-e parent glasses. Half-sphere (Ths) and melting (Tm) temperatures were obtained through dilatometric analysis. Experimental coefficients of thermal expansion (α_{EXP}) were obtained from the slopes of the dilatometry plots (Fig. 7a). Theoretical coefficients of thermal expansion (α_T) were calculated through Eq. A and experimental chemical compositions of LAS-s and LAS-e (Table III). Densities values were obtained by He-picnometry. The variations among α_{EXP} and α_T can be attributed especially to temperature range analyzed for each one. Experimental data for calculation of α_{EXP} were recorded only from 100 ºC due to the limitation of equipment while α_T calculated from Appen method took into account thermal expansion from 25 ºC. Table III shows the theoretical and the experimental chemical composition of LAS-s and LAS-e parent glasses. An excess of 2 wt% of Li_2O was added to compensate the frequently reported Li volatilization during

Table II - Measured thermal and physical properties on LAS-s and LAS-e parent glass samples.
[Tabela II - Propriedades térmicas e físicas medidas em amostras dos precursores vitrocerâmicos LAS-s e LAS-e.]

Property	LAS-s	LAS-e
Tg (°C)	618	575
Ts (°C)	685	619
Tc (°C)	795	737
Ths (°C)	1313	1324
Tm (°C)	1324	1322
Appen, α_T, 25-400 °C (10^{-6} °C^{-1})	8.07	9.33
Experimental, α_{EXP}, 100-400 °C (10^{-6} °C^{-1})	9.09	11.13
Density (g.cm^{-3})	2.44	2.49

Table III - Theoretical and experimental chemical composition (wt%) of LAS-s and LAS-e parent glasses.
[Tabela III - Composições químicas calculadas e experimentais (% em massa) dos precursores vitrocerâmicos LAS-s e LAS-e.]

Oxide	LAS-s		LAS-e	
	Theor.	Experim.	Theor.	Experim.
SiO_2	59.5	56.6	45.3	47.7
Al_2O_3	24.8	24.3	36.0	29.5
Li_2O	7.7	10.4	11.2	13.6
TiO_2	2.3	3.0	2.3	2.8
ZrO_2	1.8	1.9	1.8	2.3
Fe_2O_3	0.8	1.0	0.7	1.2
Na_2O	1.0	0.8	0.6	0.7
B_2O_3	0.4	0.5	0.1	0.5
K_2O	0.8	0.5	<0.1	0.5
CaO	0.2	0.3	<0.1	0.4
P_2O_5	0.2	0.2	<0.1	0.1
MgO	0.2	0.1	<0.1	0.2
LOI	-	0.4	-	0.6

Note: BaO, Co_2O_3, Cr_2O_3, PbO, ZnO, MnO, SrO <0.1%.

glass melting in temperatures above 1300 °C. However, the loss was not observed for any of the produced parent glasses. The final compositions of the glasses were slightly shifted from the originally designed composition. Analyzing the molar ratios of the ternary system for LAS-s with 1:1:4 ratio, the theoretical (calculated) variability was ±0.19. The experimentally observed variability was ±1.3, caused by the excess of non-volatilized Li_2O. This difference may be critical and prevent the crystallization of β-spodumene structure. On the other hand, the analysis error of ±1% by mass should also be taken into account. LAS-e was calculated based on the stoichiometry of β-eucryptite, with a

1:1:2 molar ratio. The theoretical variability was ±0.1 while the experimental variability was ±0.7. LAS-e presented an Al_2O_3 content 6.5 wt% lower than the designed composition.

To verify the mechanism of crystallization, viscosity curves were calculated using the VFT model, as shown in Fig. 8. At the crystallization temperatures, the viscosities of LAS-s and LAS-e were found to be within the range of volume crystallization for the curve calculated with T_3=Ths (Fig. 8a). For LAS-s, the crystallization viscosity was also found to be within the range of volume crystallization for the curve calculated with T_3=Tm (Fig. 8b), but for LAS-e the viscosity according to this second curve was slightly lower than the typical expected for volume crystallization. Nevertheless, the crystallization viscosity was not low enough to indicate surface crystallization. Table IV shows the kinetics parameters of crystallization obtained by DSC measurements. In good agreement with the viscosity approach, the Avrami index n, calculated through the Jeziorny modification, also indicated volume crystallization with n>2 in all conditions. Furthermore, from the obtained n-values it can be inferred that LAS-e crystals grew in two dimensions (n~3), while in LAS-s crystal growth changed from 2-D (n~3) to 1-D (n~2) at higher heating rates. The apparent activation energy was lower for LAS-e, with crystallization occurring at a lower temperature. The nucleation trends are shown in Fig. 9. The qualitative plot indicated that the highest nucleus concentration was

Table IV - Crystallization kinetic parameters of the parent glasses, LAS-s and LAS-e.
[Tabela IV - Parâmetros cinéticos de cristalização dos precursores vitrocerâmicos, LAS-s e LAS-e.]

Glass	Φ (°C.min^{-1})	T_P (°C)	ΔH (J.g^{-1})	n	E_a (kJ.mol^{-1})
LAS-s	5	779	65	3.30±0.18	337±2
	10	795	72	3.04±0.06	
	15	807	84	2.88±0.09	
	20	817	79	2.83±0.05	
LAS-e	5	700	115	2.94±0.05	205±6
	10	737	98	2.97±0.09	
	15	737	100	3.02±0.03	
	20	748	102	2.96±0.03	

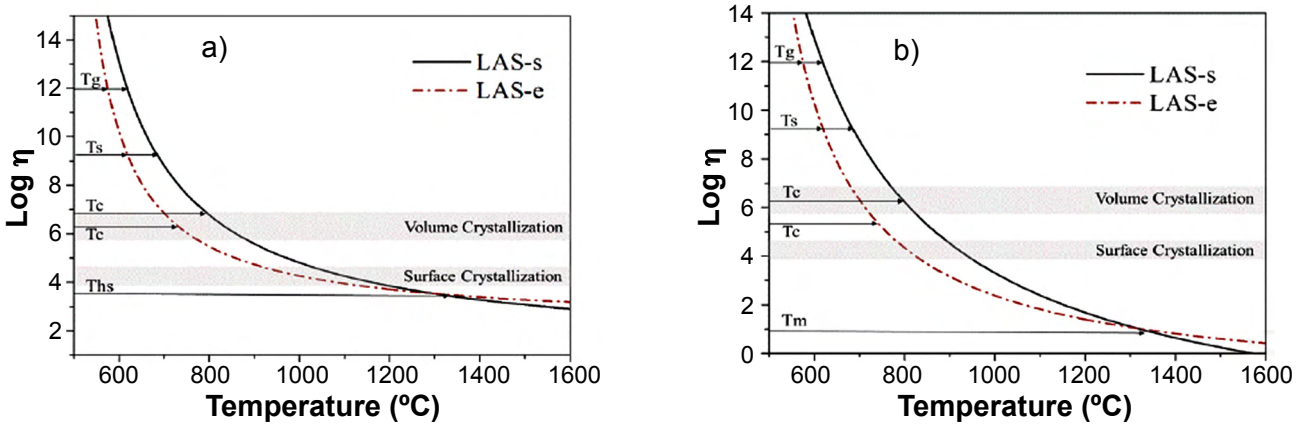

Figure 8: Viscosity vs. temperature curves calculated from the VFT equations for: a) T_3=Ths; and b) T_3=Tm.
[Figura 8: Curvas de viscosidade em função da temperatura calculadas com o auxílio das equações de VFT para: a) T_3=Ths; e b) T_3=Tm.]

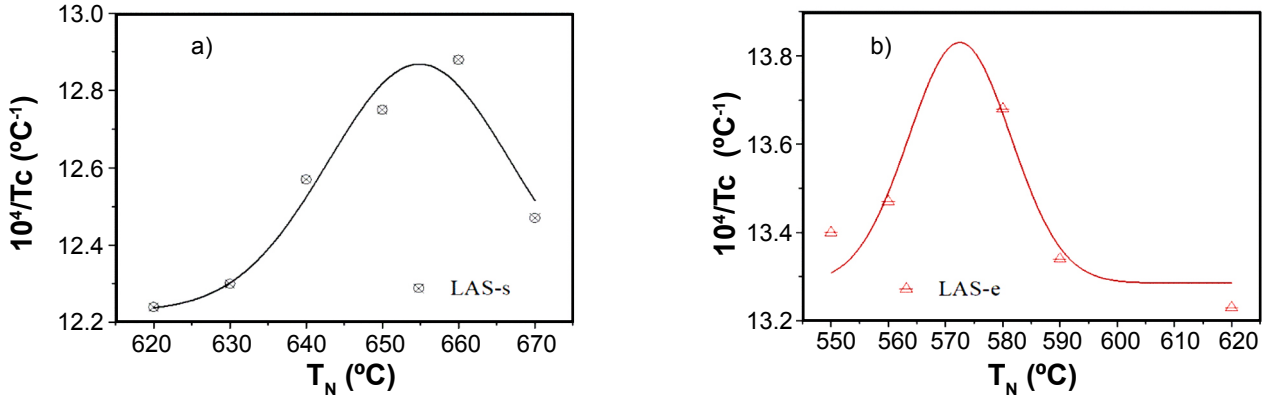

Figure 9: Nucleus concentration trends obtained from the plot of the inverse of crystallization temperature (10^4/Tc) vs. nucleation temperature (T_N).
[Figura 9: Tendências de concentração de núcleos obtidas a partir da curva do inverso da temperatura de cristalização (10^4/Tc) em função da temperatura de nucleação (T_N).]

achieved at around 655 °C for LAS-s (Fig. 9a) and 575 °C for LAS-e (Fig. 9b). Those temperatures were fixed as the nucleation temperature for the heat-treatment for 120 min (first step) to produce a higher crystalline fraction. Different crystallization temperatures were used with holding time of 120 min (second step) to evaluate crystal growth and microstructure evolution.

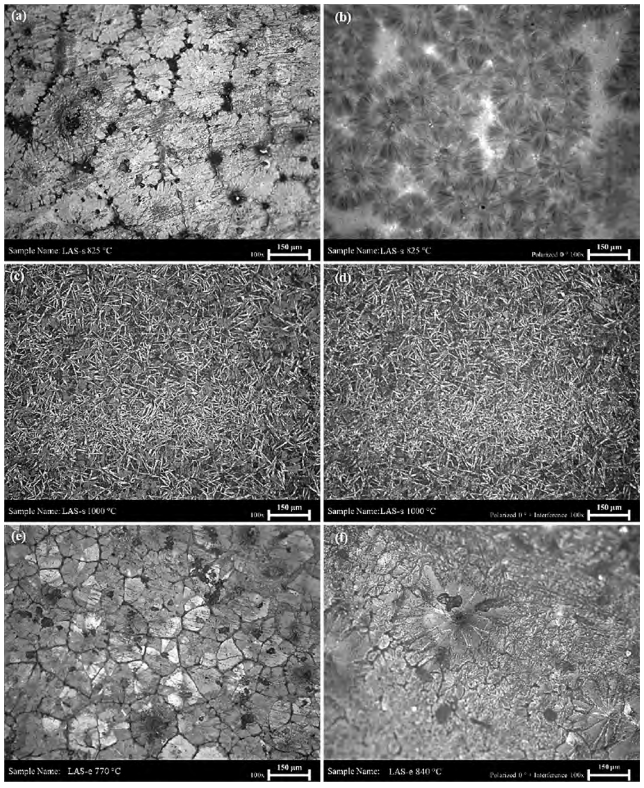

Figure 10: Optical micrographs of glass-ceramic free surfaces without chemical etching: a) LAS-s 655/825 °C; b) LAS-s 655/825 °C with polarized light (0°); c) LAS-s 655/1000 °C; d) LAS-s 655/1000 °C with polarized light (0°); e) LAS-e 575/770 °C; and f) LAS-e 575/770 °C with polarized light (0°) and interference.
[Figura 10: Micrografias ópticas das superfícies livres de amostras de vitrocerâmicas sem ataque químico: a) LAS-s 655/825 °C; b) LAS-s 655/825 °C com luz polarizada (0°); c) LAS-s 655/1000 °C; d) LAS-s 655/1000 °C com luz polarizada (0°); e) LAS-e 575/770 °C; e f) LAS-e 575/770 °C com luz polarizada (0°) e interferência.]

Optical micrographs in Fig. 10 show the microstructure aspect of LAS-s and LAS-e samples subject to different heat-treatments for nucleation and crystallization (crystal growth). Fig. 10a shows plate-shaped crystals for LAS-s heat-treated at 655/825 °C. In Fig. 10b the same region is seen with polarized light (0°). The image allowed to infer that crystals grew radially from the center, as reported in the literature for β-quartz$_{ss}$ [26]. Increasing the temperature (Figs. 10c and 10d), rod-shaped crystals grew in the sample heat-treated at 655/1000 °C, suggesting the transformation of β-quartz$_{ss}$ to β-spodumene$_{ss}$. The evolution of LAS-s microstructure with temperature seemed to be in good agreement with the designed compositions within the pseudo-ternary system Li_2O-Al_2O_3-SiO_2 (Fig. 2) and the obtained n-values. The microstructures resulting from the LAS-e heat-treated at 575/770 °C (Fig. 10e) and at 575/840 °C (Fig. 10f) exhibited crystals similar to those observed in LAS-s heat-treated at 655/825 °C. The micrograph shown in Fig. 10f was obtained with polarized light (0°) and interference to observe the surface. A central nucleus is apparent in the center, which was probably the nucleating agent zirconium titanate acting as an interface for crystal growth. The crystallization heat-treatment at a higher temperature (840 °C) did not significantly affect the nature of crystal growth but resulted in a slight growth of these β-quartz crystals.

LAS-s crystalline phases were identified by XRD as shown in Fig. 11. The β-quartz→β-spodumene transformation began at temperatures as low as 825 °C and it was not completed at 1000 °C. The intensity of peaks of β-spodumene increased with temperature while the peak intensity close to the reference β-eucryptite decreased. The most intense peak did not grow at the same rate. However, the overlap of β-spodumene and β-eucryptite main peaks was the probable reason for that effect. Despite the Li_2O excess observed in the AAS and XRF analyzes, the microstructure

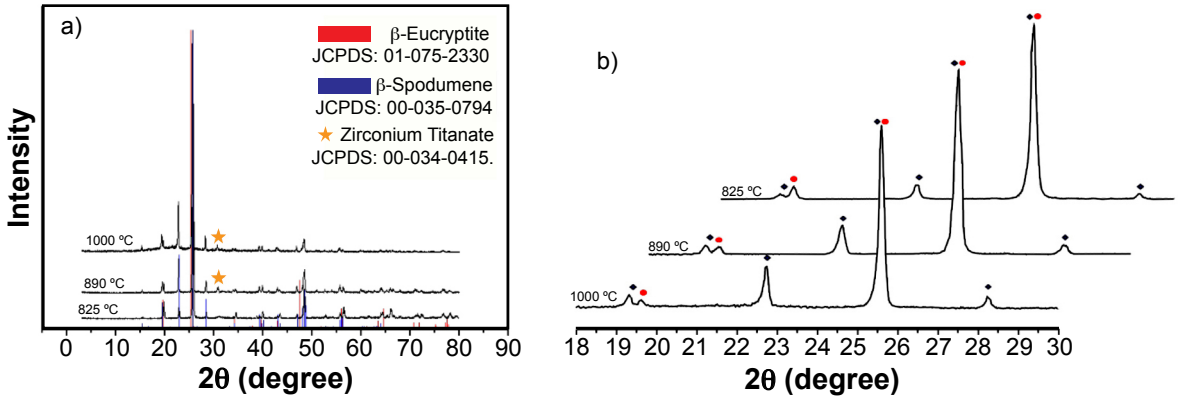

Figure 11: XRD patterns of LAS-s heat-treated at 655/825, 655/890 and 655/1000 °C (a), and pattern details in the range 18°<2θ<30° (b).
[Figura 11: Padrões de DRX das vitrocerâmicas LAS-s tratadas termicamente a 655/825, 655/890 e 655/1000 °C (a) e detalhes da região 18°<2θ<30° (b).]

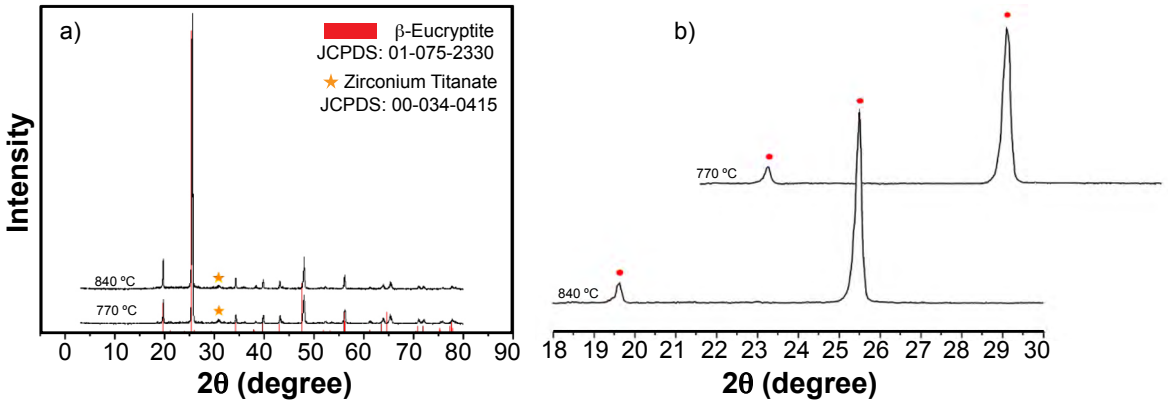

Figure 12: XRD patterns of LAS-e heat-treated at 575/770 and 655/840 °C (a), and pattern details in the range 18°<2θ<30° (b).
[Figura 12: Padrões de DRX das vitrocerâmicas LAS-e tratadas termicamente a 575/770 e 655/840 °C (a) e detalhes da região 18°<2θ<30° (b).]

evolution with temperature was as expected for the calculated composition. The most intense peak of zirconium titanate (JCPDS 00-034-0415) occurred at 2θ=30.44° and it was not overlapped by any of characteristic peaks of β-spodumene and β-eucryptite. This peak was observed in samples heat-treated at higher temperatures. The precipitates acted in the glass matrix as a nucleating agent. This may also be seen in the LAS-e XRD pattern in Fig. 12. In all cases, the increase in temperature caused the shift of the main peaks to lower 2θ, characteristic of the crystal growth. Even at lower treatment temperatures, the peaks were found to be at a lower 2θ, when compared to the reference. Besides crystal growth with temperature, the presence of the magnesium, sodium and potassium oxides in the SC composition may have led to a partial replacement of the lithium atoms in the structure, increasing the crystallite size.

The potential for thermal shock resistance of this glass-ceramics was determined from the coefficients of thermal expansion (α) obtained by the angular coefficient on the contact dilatometry curve between 100 and 700 °C (Table V). According to the unified theory for thermal shock by Hasselman [48], the parameter R predicts the behavior of resistance to thermal shock damage of fragile material. The parameters R, R' and R" determine the minimal thermal shock required to initiate a crack (each under different thermal stress conditions). The parameters R"' and R"" express the resistance to damage propagation caused by thermal shock. To exemplify, the thermal shock behavior described by the parameters R and R"' are given in Eqs. L and M:

$$R = \frac{\sigma_f(1-\upsilon)}{\alpha E} \quad \text{(L)}$$

$$R''' = \frac{E}{\sigma_f^2(1-\upsilon)} \quad \text{(M)}$$

in which R is the maximum permissible temperature variation in case of abrupt change of surface temperature before the start of the crack, E is Young's modulus, σ_f the fracture stress and υ is Poisson's ratio and, after the crack is initiated, the parameter R"' determines the minimum elastic energy for crack propagation leading to a catastrophic fracture. Analyzing Eqs. L and M, the role of E and σ_f on the material behavior under thermal shock is reversed prior and after the crack initiation. Therefore, modeling the behavior to thermal shock by increasing or decreasing E or σ_f can have detrimental effects either increasing the risk of a catastrophic rapid failure or hindering the temperature difference supported by the material before the crack starts. The coefficient of thermal expansion, α, on the other hand, has no influence on the minimum energy for crack propagation. Hence, the closer to zero the value of α, the greater is the resistance to abrupt temperature variation of a material, without directly affecting its catastrophic failure behavior.

For LAS-s glass-ceramics, values of α in the 3.524 to 4.501 x10^{-6} °C^{-1} range were obtained. The coefficient of thermal expansion, α, increased with the increase of crystallization temperature. This phenomenon can be related to the transformation of β-quartz (with a lower α) into β-spodumene (which has a higher α) as observed in the micrographs and XRD patterns. The LAS-e glass-ceramic composition was designed close to the stoichiometry of the β-eucryptite phase, which presented slightly negative α. The obtained α ranged from -0.370 to 2.351 x10^{-6} °C^{-1}, decreasing with the increase of treatment temperature, which

Table V - Coefficients of thermal expansion (α) obtained for the glass-ceramics LAS-s and LAS-e.
[Tabela V - Coeficientes de expansão térmica linear (α) obtidos para as vitrocerâmicas LAS-s e LAS-e.]

Sample	T_N (°C)	T_C (°C)	$\alpha_{(100\text{-}700\ °C)}$ (10^{-6} °C^{-1})
LAS-s	655	825	3.524±0.004
	655	895	4.265±0.005
	655	1000	4.501±0.005
LAS-e	575	770	2.351±0.003
	575	840	-0.370±0.012

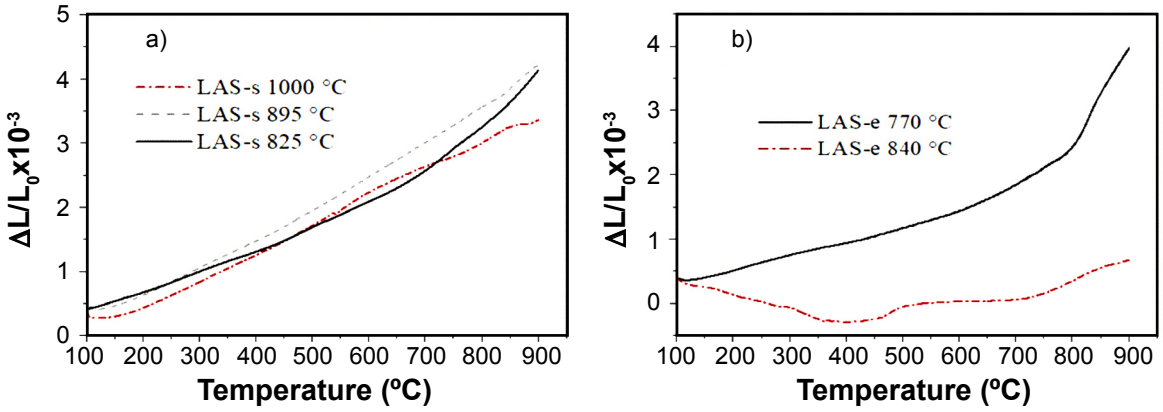

Figure 13: Linear thermal expansion curves of: a) LAS-s samples heat-treated at 655/825, 655/890 and 655/1000 °C; and b) LAS-e samples heat-treated at 575/770 and 655/840 °C.

[Figura 13: Curvas de expansão térmica linear de: a) amostras de LAS-s tratadas a 655/825, 655/890 e 655/1000 °C; e b) amostras de LAS-e termicamente tratadas a 575/770 e 655/840 °C.]

might be associated with a higher β-quartz$_{ss}$ crystalline content. In Fig. 13a, it is possible to observe that α values were almost constant up to 900 °C for LAS-s but increased significantly above 800 °C for LAS-e (Fig. 13b). The relative linearity of the LAS-s expansion curve indicated certain thermal stability of β-spodumene phase up to 900 °C. LAS-e, on the other hand, showed an abrupt change on thermal expansion behavior at around 800 °C, limiting its maximum service temperature to 700 °C. While LAS-s had a relative lower thermal-shock performance compared to LAS-e, its maximum service temperature was higher.

Some attempts to obtain the glass-ceramic of the LAS system from mineral spodumene are found in the literature, with Australian [25] and Portuguese [49] minerals. Both studies obtained monolithic glass-ceramics and reported the need for a nucleating agent to promote the volume crystallization. Color limitation and eventual non-homogeneity after the crystallization treatment were also observed. The glass-ceramic obtained from the Australian spodumene presented β-quartz$_{ss}$ and β-spodumene$_{ss}$ crystals, but the published paper did not report the obtained coefficient of thermal expansion. The α of the Portuguese glass-ceramic was found to be between 0.63 and 2.34 x10^{-6} °C^{-1} measured up to 300 and 500 °C, respectively.

CONCLUSIONS

Brazilian spodumene concentrate was successfully used to produce thermal shock resistant glass-ceramic in the LAS (Li_2O-Al_2O_3-SiO_2) system. Authors expect to call the attention of companies and government regarding the potential of spodumene concentrate being used as a lithium bearing raw material in the manufacture of glass-ceramics. The observed microstructural control and low coefficients of thermal expansion values (in the range -0.370 to 4.501 x10^{-6} °C^{-1}) provide encouraging evidences for the application of Brazilian spodumene as raw material for the production of glass-ceramics of LAS system.

ACKNOWLEDGMENT

Authors are grateful to MCTI/CNPq/CT-Mineral Nº 51/2013 (Proc. 407032/2013-4) for funding this work.

REFERENCES

[1] U.S. Geolog. Survey, Min. Commod. Summar. 2016, U.S. Dept. Interior, USA (2017).
[2] U.S. Geolog. Survey, Min. Commod. Summar. 2015, U.S. Dept. Interior, USA (2016).
[3] U.S. Geolog. Survey, Min. Commod. Summar. 2014, U.S. Dept. Interior, USA (2015).
[4] U.S. Geolog. Survey, Min. Commod. Summar. 2013, U.S. Dept. Interior, USA (2014).
[5] U.S. Geolog. Survey, Min. Yearbook 2015, U.S. Dept. Interior, USA (2017) 2.
[6] R.L.G. Reis, Rev. Miner. **328** (2013) 46.
[7] P.F.A. Braga, J.A. Sampaio, "Rochas & minerais industriais: usos e especificações", CETEM, Rio Janeiro (2008) 603.
[8] Subchef. Assunt. Juríd., Consel. Presid. Repúbl., Casa Civil, Decreto Nº 2413 (1997).
[9] I.J. Garcia, Sumár. Miner., Depto. Nac. Produç. Miner. **34** (2014) 82.
[10] P. Braga, S. França, C. Junior, in Proc. XXVII Int. Miner. Proc. Congr., Santiago (2014) 442.
[11] CNEN, Portaria Nº 279 (1997).
[12] P.N. Belmiro, Lubes Foco **55** (2016) 6.
[13] S. Arcaro, M. Isabel Nieto, J.B. Rodrigues Neto, A.P.N. de Oliveira, R. Moreno, J. Am. Ceram. Soc. **99** (2016) 3573.
[14] S. Arcaro, B. Moreno, E. Chinarro, M.D. Salvador, A. Borrell, M.I. Nieto, R. Moreno, A.P.N de Oliveira, J. Alloy. Compd. **710** (2017) 567.
[15] F.R. Cesconeto, S. Arcaro, F. Raupp-Pereira, J.B. Rodrigues Neto, D. Hotza, A.P.N. de Oliveira, Ceram. Int. **40**, (2014) 9535.
[16] O.R.K. Montedo, P.C. Milak, F.D. Minatto, R.B.

Nuernberg, C.A. Faller, A.P.N. de Oliveira, J. Therm. Anal. Calorim. **124** (2016) 241.
[17] R.B. Nuernberg, C.A. Faller, O.R.K. Montedo, J. Therm. Anal. Calorim. **127** (2017) 355.
[18] Z. Zhang, B. Wang, H. Gong, Z. Gu, Y. Liu, in Proc. Int. Symp. Optoelectr. Technol. Appl., Imag. Spectrosc. Telescop. Large Optics, J.P. Rolland, C. Yan, D.W. Kim, W. Ma, L. Zheng (Eds.), Beijing (2014) 929818.
[19] D. Krause, H. Bach, *Low thermal expansion glass ceramics*, Springer-Verlag, Germany (2005) 121.
[20] S. Buchner, V.O. Soares, P. Soares, C.M. Lepienski, E.D. Zanotto, Glass Technol.-Part A **54** (2013) 211.
[21] E. Kleebusch, C. Patzig, M. Krause, Y. Hu, T. Höche, C. Rüssel, Sci. Rep. **8** (2018) 2929.
[22] W. Pannhorst, Glass Technol. Eur. J. Glass Sci. Technol. **45** (2004) 51.
[23] O. García-Moreno, W.M. Kriven, J. S. Moya, R. Torrecillas, J. Am. Ceram. Soc. **96** (2013) 2039.
[24] U. Scheithauer, E. Schwarzer, T. Moritz, A. Michaelis, J. Mater. Eng. Perform. **27** (2018) 14.
[25] A. Nordmann, Y.-B. Cheng, J. Mater. Sci. **32** (1997) 83.
[26] Z. Strnad, *Glass-ceramic materials: liquid phase separation, nucleation and crystallization in glasses*, Elsevier, Czechoslovakia (1986).
[27] M. Chavoutier, D. Caurant, O. Majérus, R. Boulesteix, P. Loiseau, C. Jousseaume, E. Brunet, E. Lecomte, J. Non-Cryst. Solids **384** (2014) 15.
[28] K. Cheng, Mater. Sci. Eng. B **60** (1999) 194.
[29] C. S. Rao, V. Ravikumar, T. Srikumar, Y. Gandhi, N. Veeraiah. J. Non-Cryst. Solids **357** (2011) 3094.
[30] X. Guo, H. Yang, C. Han, F. Song, Ceram. Int. **33** (2007) 1375.
[31] E. Kleebusch, C. Patzig, T. Höche, C. Rüssel, Ceram. Int. **43** (2017) 9769.
[32] S. Barbi, P. Miselli, C. Siligardi, Ceram. Int. **43** (2017) 1472.
[33] V. Maier, G. Müller, J. Am. Ceram. Soc. **70** (1987) 176.
[34] C.S. Ray, D.E. Day, Thermochim. Acta **280-281** (1996) 163.
[35] J.M.F. Navarro, *El vidrio*, CSIC, Spain (1991) 395.
[36] D. Ovono, S. Berre, P. Pradeau, M. Comte, G. Bruno, Thermochim. Acta **527** (2012) 158.
[37] H. Vogel, Physikal. Zeitschr. **22** (1921) 645.
[38] G. Tammann, W. Hesse, Z. Anorg. Allg. Chem. **156** (1926) 247.
[39] C.P. Martendal, A.P.N. de Oliveira, J. Therm. Anal. Calorim. **130** (2017) 1903.
[40] E. Neves, E.D. Poffo, M.C. Fredel, H.G. Riella, O.E. Alarcon, Quim. Nova **21** (1998) 534.
[41] M. Avrami, J. Chem. Phys. **7** (1939) 1103.
[42] A. Jeziorny, Polymer **19** (1978) 1142.
[43] S. Thomas, M. Arif, E.B. Gouwd, N. Kalarikkal, *Crystallization in multiphase polymer systems*, Elsevier, UK (2017) 524.
[44] H.E. Kissinger, J. Res. Nat. Bur. Stand. **57** (1956) 217.
[45] C.S. Ray, D.E. Day, J. Am. Ceram. Soc. **73** (1990) 439.
[46] G.H. Beall, Int. J. Appl. Glass Sci. **5** (2014) 93.
[47] Q.A. Acton, "Lanthanide series elements - advances in research and application", Schol. Ed., USA (2013) 116.
[48] D.P.H. Hasselman, J. Am. Ceram. Soc. **52** (1969) 600.
[49] D.U. Tulyaganov, S. Agathopoulos, H.R. Fernandes, J.M.F. Ferreira, Ceram. Int. **30** (2004) 1023.
(Rec. 17/08/2018, Rev. 17/12/2018, 21/01/2019, Ac. 10/02/2019)